Evolution from a heavy-fermion metal to an antiferromagnetic insulator in the *A*-site ordered perovskite $PbCu_3Ru_{4-x}Ti_xO_{12}$

Ruifeng Tian,[1] Jie Chen,[1,*] Feng Wu,[1,2] Jiayi Guan,[1,3] Zhiyan Shao,[1] Wei Wu,[2] Mingwei Ma,[2] Zhiwei Hu,[4] Haoyu Zheng,[2] Pengda Ye,[1,5] Yuxiang Chen,[1] Hua Zhang,[2] Yanfeng Guo,[6] Meiling Jin,[1,†] Jiabin Qiao,[1,‡] Fan Yang,[1,§] and Xiang Li[1,‖]

[1]*Key Lab of Advanced Optoelectronic Quantum Architecture and Measurement (MOE) and School of Physics, Beijing Institute of Technology, Beijing 100081, People's Republic of China*

[2]*Institute of Physics, Chinese Academy of Sciences, Beijing 100091, People's Republic of China*

[3]*Center for High Pressure Science and Technology Advanced Research (HPSTAR), Shanghai 201203, People's Republic of China*

[4]*Max-Planck-Institute for Chemical Physics of Solids, 01187 Dresden, Germany*

[5]*Key Laboratory of Biomimetic Robots and Systems, Ministry of Education, State Key Laboratory of Intelligent Control and Decision of Complex System, and School of Mechatronical Engineering, Beijing Institute of Technology, Beijing 100081, People's Republic of China*

[6]*State Key Laboratory of Quantum Functional Materials, School of Physical Science and Technology and ShanghaiTech Laboratory for Topological Physics, ShanghaiTech University, Shanghai 201210, People's Republic of China*

(Received 4 November 2025; revised 11 January 2026; accepted 13 January 2026; published 10 February 2026)

Materials tunable between heavy-fermion metals and antiferromagnetic insulators near quantum criticality are promising candidates for exploring unconventional superconductivity, yet such a behavior is rare in transition metal oxides. Here, we report the high-pressure synthesis and characterization of two Pb-based *A*-site ordered perovskites, $PbCu_3Ru_4O_{12}$ and $PbCu_3Ti_4O_{12}$, which are characterized as a heavy-fermion metal and an antiferromagnetic insulator, respectively. Systematic *B*-site substitution in $PbCu_3Ru_{4-x}Ti_xO_{12}$ ($x = 0$–4) reveals a continuous evolution of electronic and magnetic properties, with intermediate compositions exhibiting divergent low-temperature specific heat, indicative of proximity to a quantum critical point. The experimental observation supported by density functional theory calculations reveal that $PbCu_3Ru_4O_{12}$ exhibits more enhanced effective mass than $CaCu_3Ru_4O_{12}$, attributed to its enhanced Fermi-level density of states and narrower bandwidth, driven by the elongated Ru-O bonds and the covalent character of Pb^{2+}. These results establish $PbCu_3Ru_{4-x}Ti_xO_{12}$ as a rare platform to study quantum criticality and strong correlations in transition-metal oxides and demonstrate that combine *A*-site and *B*-site tuning provides an effective route to tailor electronic and magnetic properties.

DOI: 10.1103/hdnd-sd52

I. INTRODUCTION

The quest to understand unconventional superconductivity has made heavy-fermion systems a key area of materials science and condensed-matter physics, inspiring the exploration of new compounds that host heavy-fermion behavior. The physics of heavy-fermion behavior has been extensively studied in rare-earth and actinide intermetallics, where the hybridization between localized f electrons and conduction bands generates heavy quasiparticles. Rare-earth-based heavy-fermion metals have enabled experimental access to quantum critical points (QCPs), particularly antiferromagnetic QCPs, as demonstrated in $CeCu_{6-x}Au_x$ and $YbRh_2Si_2$ [1–3]. These discoveries provide an essential platform for understanding both Landau Fermi-liquid behavior and deviations leading to non-Fermi-liquid states. Furthermore, proximity to QCP often gives rise to emergent quantum phases, offering a potential route to unconventional superconductivity [4].

Theoretical studies predict that heavy-fermion behavior can also emerge in transition-metal oxides near a metal-insulator transition, however, experimental realizations remain scarce [5]. To date, only a few compounds, such as LiV_2O_4 and $Pr_2Ir_2O_7$, have been reported to exhibit heavy-fermion properties [6,7]. The dual nature of d-electrons in LiV_2O_4, acting simultaneously as localized moments and conduction carriers, makes it difficult to disentangle the origin of mass enhancement. *A*-site ordered perovskites with the formula $AA'_3B_4O_{12}$ offer a unique platform, as they enable the simultaneous incorporation of transition-metal ions at the *A*, *A*′, and *B* sites. Notably, compounds such as $CaCu_3Ru_4O_{12}$ and $CaCu_3Ir_4O_{12}$, in which the *B* site hosts $4d$ or $5d$ transition metals, display signatures of heavy-fermion behavior [8,9]. However, it remains unclear whether the underlying mechanism is analogous to that of conventional f-electron heavy-fermion systems. Moreover, access to a QCP in these *A*-site ordered perovskite heavy-fermion metals has not yet been demonstrated.

The metallic compound $CaCu_3Ru_4O_{12}$ has been proposed as a heavy-fermion system due to its striking resemblance to $4f$-electron systems. Its magnetic susceptibility is two orders

*Contact author: jiechen.phy@bit.edu.cn
†Contact author: jinml@bit.edu.cn
‡Contact author: jiabinqiao@bit.edu.cn
§Contact author: yangfan_blg@bit.edu.cn
‖Contact author: xiangli@bit.edu.cn

of magnitude higher than that of free electrons, exhibits a broad maximum as a function of temperature, and its Sommerfeld coefficient is enhanced by a factor of 20–30 compared with a conventional metal [10]. Subsequent studies by Tanaka *et al.* revealed that $NaCu_3Ru_4O_{12}$ and $LaCu_3Ru_4O_{12}$ also display enhanced Sommerfeld coefficients, with $LaCu_3Ru_4O_{12}$ exceeding that of $CaCu_3Ru_4O_{12}$ [11]. Resonant X-ray emission spectroscopy further demonstrated a systematic increase in the number of O $2p$ holes from La to Ca to Na, and suggested that the hole doping suppresses the enhancement of specific heat [12]. More recently, the presence of localized Cu^{2+} moments hybridized with itinerant electrons was deduced from hard and soft X-ray spectroscopy measurements, supporting a Kondo-lattice interpretation for $CaCu_3Ru_4O_{12}$ [13]. However, nuclear magnetic resonance (NMR) measurements detected no local moment up to 700 K, posing a serious challenge to the Kondo scenario [14]. To date, no decisive conclusions have been reached regarding the unusual properties of $CaCu_3Ru_4O_{12}$. While the microscopic origin of its unconventional heavy-fermion behavior remains debated, the interplay between Ru 4d and Cu 3d orbitals clearly plays a central role.

Substitution at the B site in A-site ordered perovskite leads to dramatically different physical properties. $CaCu_3Fe_4O_{12}$ undergoes a metal-insulator transition that is coupled with a paramagnetic-to-ferrimagnetic transition, involving charge disproportionation from Fe^{4+} to Fe^{3+} and Fe^{5+}. Neutron diffraction and X-ray magnetic circular dichroism measurements reveal that ferromagnetic Cu^{2+} spins antiferromagnetically coupled with Fe^{3+} and Fe^{5+}, giving rise to a ferrimagnetic spin structure [15]. $CaCu_3Mn_4O_{12}$ is a semiconductor with a ferromagnetic transition at 355 K and exhibits colossal magnetoresistance without mixed Mn valency [16]. $CaCu_3Co_4O_{12}$ and $CaCu_3Cr_4O_{12}$ host Zhang-Rice singlets, reflecting strong Cu–O hybridization that is tuned by the B-site cation [17]. When B-site ions are nonmagnetic p-block elements such as Ge or Sn, $CaCu_3Ge_4O_{12}$ and $CaCu_3Sn_4O_{12}$ exhibit ferromagnetic ordering via direct Cu^{2+} exchange [18]. In contrast, Ti 3d orbitals in $CaCu_3Ti_4O_{12}$ enable antiferromagnetic superexchange interactions, resulting in G-type antiferromagnetic order confirmed by neutron scattering [19]. As discussed above, a wide range of A-site ordered perovskite oxides with different B-site cations have been synthesized and studied. However, the choice of A-site ions has been largely limited to Ca^{2+} and Cu^{2+}. As widely observed in simple perovskites, the A-site ion also plays a crucial role in determining both the structure and the physical properties.

In this study, we synthesized two new Pb-based A-site ordered perovskites, $PbCu_3Ru_4O_{12}$ and $PbCu_3Ti_4O_{12}$. Detailed structural and physical characterizations, supported by density functional theory (DFT) calculations, reveal Stoner enhancement in heavy-fermion metal $PbCu_3Ru_4O_{12}$ and antiferromagnetic insulating behavior in $PbCu_3Ti_4O_{12}$. Solid solutions $PbCu_3Ru_{4-x}Ti_xO_{12}$ ($x = 1.2$, 2.0, 2.8, 3.6) were synthesized successfully, among which the $x = 1.2$ and 2.0 compositions exhibit a low-temperature upturn in specific heat and unusual electron-transport properties, suggesting proximity to a QCP. These findings demonstrate a B-site-substitution-driven transition from a heavy-fermion metal to an antiferromagnetic insulator in an A-site ordered perovskite, establishing this system as a rare platform for exploring quantum criticality and electron correlations in 3d-4d hybrid transition-metal oxides.

II. MATERIALS AND METHODS

The starting materials of PbO(99.999%, Aladdin, Shanghai, China), CuO(99.9%, Aladdin, Shanghai, China), RuO_2(99.95%, Aladdin, Shanghai, China) and TiO_2(99.99%, Aladdin, Shanghai, China) powders were weighed in a stoichiometric ratio and then thoroughly mixed and ground. Polycrystalline $PbCu_3Ru_4O_{12}$ and $PbCu_3Ru_{4-x}Ti_xO_{12}$ ($x = 1.2$, 2.0, 2.8, and 3.6) were synthesized at 12 GPa and 1200 °C with a Walker-type multianvil high-pressure apparatus (LPR-1000, Max Voggenreiter, Germany). $PbCu_3Ti_4O_{12}$ was obtained at 8 GPa and 850 °C with the same apparatus. During high-pressure synthesis, the samples were maintained at the target pressure and temperature for 30 minutes before being quenched to room temperature, followed by pressure release.

Samples obtained from high-pressure synthesis were characterized by laboratory x-ray powder diffraction using a Bruker D2 Phaser diffractometer with Cu K_α radiation, as well as by synchrotron XRD at beamline BL17UM of the Shanghai Synchrotron Radiation Facility ($\lambda = 0.688$ Å). Rietveld refinements were performed using the FULLPROF software package. The grain size of pristine polycrystalline samples were determined using a Jeol JSM-IT700HR scanning electron microscope (SEM).

Samples were characterized by x-ray absorption spectroscopy (XAS). Cu K-edge XAS measurements were conducted at beamline BL17B1 of the Shanghai Synchrotron Radiation Facility. Pb L_3-edge XAS data were collected at beamline BL12B2 of SPring-8, Japan.

The field-cooling (FC) and zero-field-cooling (ZFC) of the samples were collected using a Magnetic Properties Measurement System (MPMS, Quantum Design Inc.) over the temperature range $1.8 \leqslant T \leqslant 300$ K under applied fields of 0.1 and 1 T, respectively. The isothermal magnetization (M-H) curves were collected with a sweeping field from –7 to +7 T at 2 K. The temperature dependence of electrical resistivity, specific heat, and thermoelectric power were measured using a Physical Property Measurement System (PPMS, Quantum Design Inc.). Resistivity was measured using the standard four-probe method in the range $1.8 \leqslant T \leqslant 300$ K. Specific heat measurements were performed using Apiezon-N grease for thermal contact between the polycrystal and the sample stage in the range $1.8 \leqslant T \leqslant 300$ K.

DFT calculations with on-site Coulomb interactions (DFT+U) were performed using Vienna *ab initio* simulation package (VASP) [20–22], with the projector augmented-wave (PAW) method employed to describe the pseudopotentials. Electronic correlations were treated within the generalized gradient approximation (GGA) using the Perdew-Burke-Ernzerhof (PBE) exchange potential [23]. A k-point mesh of $10 \times 10 \times 10$ was used for Brillouin zone sampling, and the plane-wave cutoff energy was set to 550 eV.

To account for electron correlations, on-site Coulomb interaction parameters were applied with $U = 4.0$ eV for the Cu 3d orbitals and $U = 3.0$ eV for the Ti 3d or-

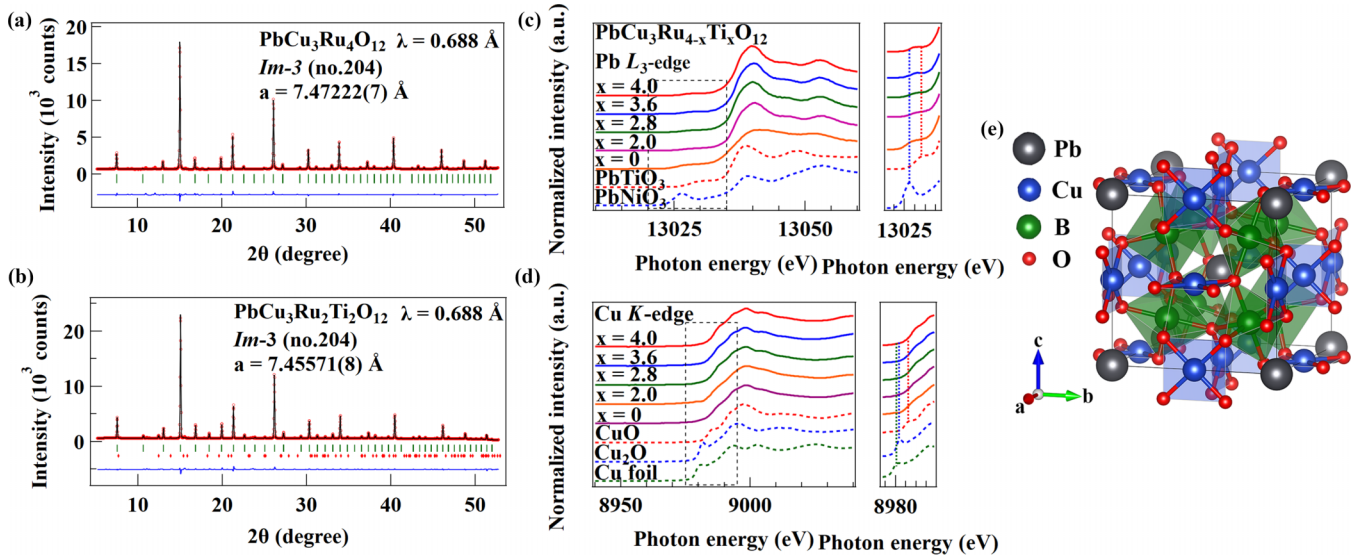

FIG. 1. The powder synchrotron XRD patterns ($\lambda = 0.688$ Å) collected at room temperature and their refinement results for (a) $PbCu_3Ru_4O_{12}$ and (b) $PbCu_3Ru_2Ti_2O_{12}$. Expected Bragg reflections are marked by ticks for the *Im*-3 structure (top) and PbO (bottom). The XAS spectra of $PbCu_3Ru_{4-x}Ti_xO_{12}$ ($x = 0$, 2.0, 2.8, 3.6, 4.0) at the (c) Pb L_3 edge and (d) Cu K edge with enlarged views of the pre-edge region. (e) Structural model for $PbCu_3B_4O_{12}$ (B = Ru, Ti).

bitals. Band structure calculations were performed using experimentally determined crystal structures and lattice parameters. For $PbCu_3Ti_4O_{12}$, a G-type antiferromagnetic ordering was considered, while non-magnetic calculations were employed for $PbCu_3Ru_4O_{12}$ and $CaCu_3Ru_4O_{12}$.

In the calculations of the γ and χ_0 based on DFT results, we use the DOS at the Fermi level excluding the contribution from Cu. This is because the Cu-derived band, which would nominally cross the Fermi level, is expected to split into two bands under strong electronic correlations–one located below and the other above the Fermi level [24,25]. However, this characteristic band splitting cannot be accurately captured by DFT+U, which tends to underestimate strong correlation effects. Therefore, in evaluating γ and χ_0, we use the $N(E_F)$, after excluding Cu contributions.

III. RESULTS

The Pb-based A-site ordered perovskite $PbCu_3B_4O_{12}$ (B = Ru, Ti) and the solid solutions $PbCu_3Ru_{4-x}Ti_xO_{12}$ (x = 1.2, 2.0, 2.8, 3.6) were synthesized under high-pressure and high-temperature conditions, as described in the Experimental section. To assess phase purity, powder x-ray diffraction (XRD) was initially performed on all the samples using Cu K_α radiation. For more detailed structural characterization, synchrotron XRD measurements were conducted at BL17UM of the Shanghai Synchrotron Radiation Facility with an incident wavelength of $\lambda = 0.688$ Å. Rietveld refinements of the synchrotron XRD patterns were carried out using the Fullprof suite. Like other A-site ordered perovskites $CaCu_3B_4O_{12}$ (B = Ti, V, Cr, Mn, Co, Ru, and Ir), a cubic structural model with space group *Im*-3 (No. 204) was adopted for Rietveld refinement. Figures 1(a) and 1(b) present the representative refinement results, with additional patterns of all the samples shown in Fig. S1 [26]. The corresponding refined structural parameters are summarized in Table S1 [26]. To determine the oxidation states of the cations, x-ray absorption spectroscopy (XAS) measurements were carried out, as shown in Figs. 1(c) and 1(d). By comparison with reference spectra, the valence states of both Pb and Cu were identified as +2. Considering the similar Ru-O bond length (1.996 Å) in $PbCu_3Ru_4O_{12}$ to those observed in $CaRuO_3$ (1.993 Å) and $SrRuO_3$ (1.986 Å) [27], along with the confirmed divalent states of Pb and Cu from XAS, the Ru ions in $PbCu_3Ru_4O_{12}$ are inferred to be +4. The divalent nature of Pb^{2+} and Cu^{2+} was further confirmed in $PbCu_3Ti_4O_{12}$ and in the solid solutions $PbCu_3Ru_{4-x}Ti_xO_{12}$ (x = 2.0, 2.8, 3.6) via XAS measurements.

The temperature dependence of resistivity $\rho(T)$, shown in Fig. 2(a), indicates that $PbCu_3Ru_4O_{12}$ remains metallic down to 2 K. The magnitude and temperature dependence of thermoelectric power (S) also support the metallic nature of this compound, as shown in Fig. 2(b). At low temperatures, the resistivity exhibits a linear dependence on T^2 at $T < 70$ K, typical for the Fermi-liquid behavior, as illustrated in the inset of Fig. 2(a). Fitting the data to the formula $\rho = \rho_0 + A \times T^2$, yields $\rho_0 = 2.70$ mΩ cm and $A = 4.30 \times 10^{-7}$ Ω cm K^{-2}. Similar Fermi-liquid behavior has been reported for $CaCu_3Ru_4O_{12}$, in which ρ is linear with T^2 over the 2–25 K range [8]. Notably, the A coefficient for $CaCu_3Ru_4O_{12}$ is 6×10^{-9} Ω cm K^{-2}, nearly two orders of magnitude smaller than that of $PbCu_3Ru_4O_{12}$. This significant enhancement in A coefficient may suggest stronger electron correlations in $PbCu_3Ru_4O_{12}$, possibly associated with a larger effective mass. It should be noted, however, that the resistivity measurements were performed on polycrystalline $PbCu_3Ru_4O_{12}$ and $CaCu_3Ru_4O_{12}$ samples, and grain-boundary effects inherent to polycrystalline materials may influence the extracted A coefficient. Therefore a definitive assessment of mass enhancement requires an analysis of the Sommerfeld coefficient (γ) derived from specific heat measurements.

The temperature dependence of specific heat (C_p) for $PbCu_3Ru_4O_{12}$ is shown in Fig. 2(c). In the low-temperature region, the data were fitted with an approximated Debye

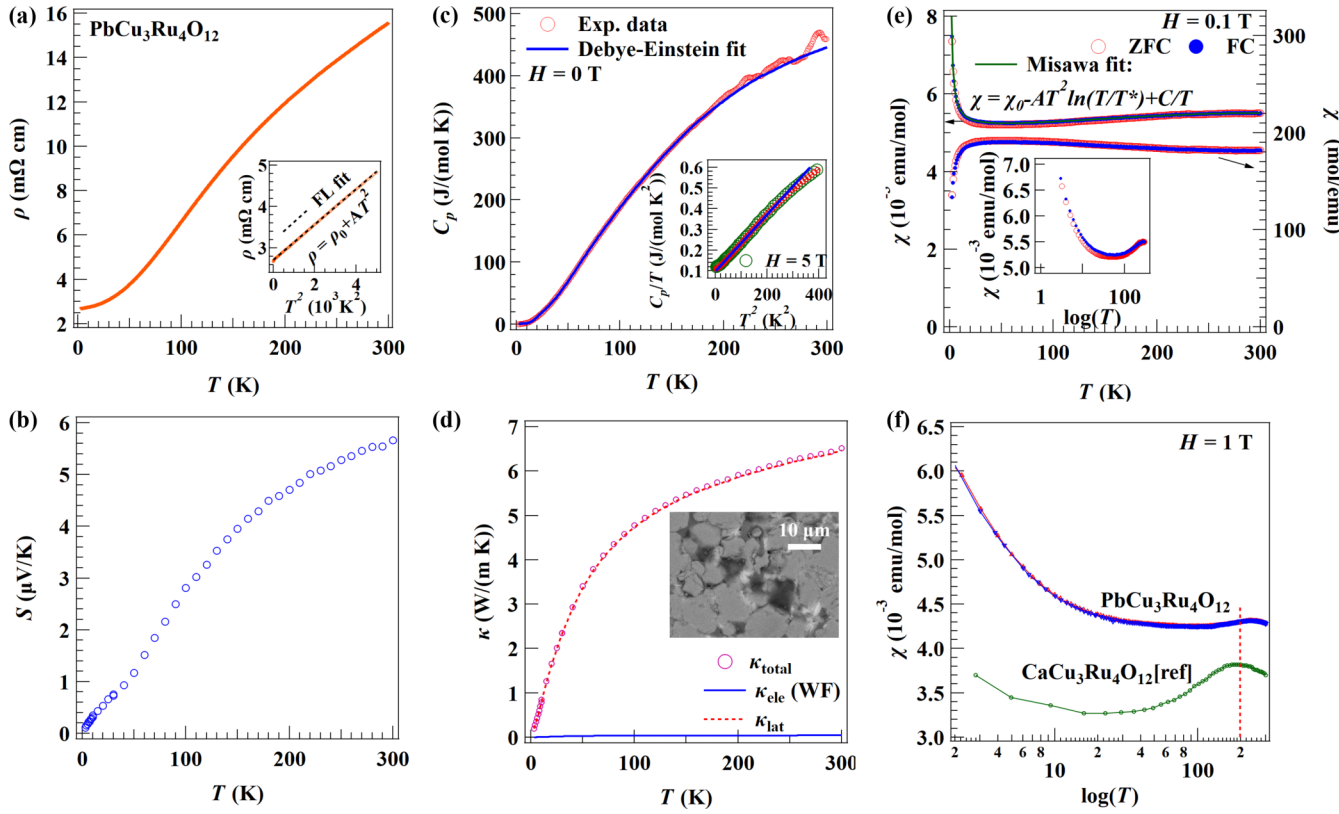

FIG. 2. Temperature dependence of (a) resistivity $\rho(T)$ at $H = 0$ T with $\rho(T^2)$ shown in the inset, (b) thermopower $S(T)$, (c) specific heat $C_p(T)$ with C_p/T versus T^2 shown in the inset, (d) thermal conductivity $\kappa(T)$ with an SEM image of polycrystalline $PbCu_3Ru_4O_{12}$ shown in the inset, (e) magnetic susceptibility $\chi(T)$ measured under $H = 0.1$ T, and (f) $\chi(T)$ measured under $H = 1$ T. The $\chi(T)$ data for $CaCu_3Ru_4O_{12}$ are reproduced from Ref. [10].

model, $C_p/T = \gamma + \beta_0 T^2$, yielding a Sommerfeld coefficient of $\gamma = 98.05$ mJ/mol K^2 and $\beta_0 = 1.37$ mJ mol^{-1} K^{-4}. The obtained γ value is larger than that of $CaCu_3Ru_4O_{12}$, previously reported as 84 [8] and 92 mJ/mol K^2 [10]. The Kadowaki-Woods ratio, A/γ^2, for $PbCu_3Ru_4O_{12}$ is estimated to be 44.8 μΩ cm mol^2 K^2 J^{-2}, which is comparable to the characteristic value of ∼ 10 μΩ cm mol^2 K^2 J^{-2} observed in the heavy-fermion systems [28]. The thermal conductivity (κ) of $PbCu_3Ru_4O_{12}$, as shown in Fig. 2(d), exhibits a glasslike behavior similar to that of $CaCu_3Ir_4O_{12}$ [9]. To estimate the electronic contribution, the Wiedemann-Franz law, $\kappa_E = L\sigma T$, where L is the Lorenz number, was applied. The calculated κ_E is negligible compared with the total thermal conductivity (κ_{total}). The average grain size of the pristine sample is about 5–10 μm [Fig. 2(d)], revealed by scanning electron microscope (SEM), much larger than the phonon mean free path, ruling out grain-boundary scattering as the origin of the glass-like behavior. The negligible κ_E appears to be consistent with the heavy-fermion scenario. In such systems, strong coupling between conduction electrons and localized magnetic moments substantially reduces electron mobility. Strong interactions between the heavy conducting electrons and the lattice vibrations further suppress $\kappa_{lattice}$.

Figures 2(e) and 2(f) present the magnetic susceptibility (χ) of $PbCu_3Ru_4O_{12}$, together with $CaCu_3Ru_4O_{12}$ for comparison. A broad maximum is clearly observed above 100 K, peaking around 275 K. This feature resembles that of $CaCu_3Ru_4O_{12}$, with the peak in $PbCu_3Ru_4O_{12}$ occurring at higher temperature. The broad maximum was initially attributed to Kondo screening, where itinerant d electrons of Ru begin to interact with localized Cu^{2+} moments [10]. However, the Kondo scenario for $CaCu_3Ru_4O_{12}$ remains controversial. The absence of local moment signature remains up to 700 K, revealed by NMR measurements [14]. Angle-resolved photoemission spectroscopy combined with theoretical simulations suggests that $3d$ electrons of Cu remains itinerant even at high temperature [29]. The LDA+DMFT calculations reproduce the local spin susceptibility at the Cu site of $CaCu_3Ru_4O_{12}$, indicating that the Kondo screening could occur in the 500–1000 K range [13]. Thus both experimental and theoretical studies provide no definitive explanation for the broad maximum in the $\chi(T)$ curve.

Alternatively, the model developed by Misawa successfully reproduces the magnetic susceptibility maximum in variety of metals near to the ferromagnetic transition [30,31]. We attempted to apply Misawa's model, $\chi = \chi_0 - AT^2 \ln(\frac{T}{T^*})$, to fit the χ(T) data. As shown in Fig. S2, the model captures the broad maximum very well. To account for the upturn at low temperature, likely due to magnetic impurities, we added a Curie term, giving $\chi = \chi_0 - AT^2 \ln(\frac{T}{T^*}) + \frac{C}{T}$. The fitting result, overlaid in Fig. 2(e), gives $\chi_0 = 4.161(2) \times 10^{-3}$ emu/mol, $A = 3.8(2) \times 10^{-9}$ emu/mol K^2, and $T^* = 434(8)$ K. The maximum temperature $T_{max} = T^*/\sqrt{e}$ (∼ 263 K),

TABLE I. Comparison of physical properties of $PbCu_3Ru_4O_{12}$ and $CaCu_3Ru_4O_{12}$.

	$PbCu_3Ru_4O_{12}$		$CaCu_3Ru_4O_{12}$	
Space group	*Im*-3			
Lattice parameter (Å)	7.47222(7)		7.4098 [8]	
$\rho = \rho_0 + AT^n$	A = 4.30×10^{-4} mΩ cm/K^2, $n = 2$		A = 2.95×10^{-5} mΩ cm/K^2, $n = 2$ [8]	
χ_0(emu/mol)	EXP	4.16×10^{-3}	EXP	3.20×10^{-3} [32]
	DFT	3.4×10^{-4}	DFT	2.3×10^{-4}
γ (mJ K^{-2} mol^{-1})	EXP	98.05	EXP	80 [32]
	DFT	25	DFT	16.85
T_{FL} (K)	70		25	
$R_{kw} = A/\gamma^2$	44.8		3.5	
$R_w = \frac{\pi^2 k_B^2 \chi}{3\mu_B^2 \mu_0 \gamma}$	3.1		2.8	

agrees well with the experimental observation. This analysis suggests that the susceptibility maximum in $PbCu_3Ru_4O_{12}$ arises from strong electron correlations and proximity to a ferromagnetic instability. We applied the same fitting to the $\chi(T)$ data of $CaCu_3Ru_4O_{12}$, which also reproduces the broad maximum, as shown in Fig. S3. The study by Kao *et al.* attributed the broad maximum in $\chi(T)$ of $CaCu_3Ru_4O_{12}$ to strong spin fluctuations, which can be revealed from its band structure [32].

The χ_0 estimated from Misawa fitting and from the fitting formula $\chi = \chi_0(1-aT^2)$ for a paramagnetic metal are consistent, show in Table I. The magnetic susceptibility χ_0 is strongly enhanced relative to the Pauli paramagnetic susceptibility derived from the DOS at Fermi energy $N(E_F)$. Our DFT calculations yield $N(E_F) = 10.58$ states/eV/f.u./spin, giving $\chi_0(\text{DFT}) = 3.4 \times 10^{-4}$ emu/mol. If the enhancement of χ_0 were solely due to mass enhancement, the ratio $\chi_0/\chi_0(\text{DFT})$ should be comparable to $\gamma/\gamma(\text{DFT})$. Using $\gamma = \frac{\pi^2}{3}k_B^2 N(E_F)$, we obtain $\gamma(\text{DFT}) = 24.94$ mJ/mol K^2. The ratios $\chi_0/\chi_0(\text{DFT})$ and $\gamma/\gamma(\text{DFT})$ are 12 and 4, respectively, indicating that the enhancement of χ_0 exceeds that of γ. This suggests an additional mechanism specifically enhancing the magnetic susceptibility. The susceptibility enhancement can be understood as arising from two contributions. The first is mass renormalization, which intrinsically enhances χ_0. The second arises from electronic correlations that further amplify the susceptibility via the Stoner mechanism, described within the random-phase approximation (RPA). The Stoner-enhanced susceptibility can be expressed as $\chi = \chi_0(1-aT^2)K_0^{-2}$, where the Stoner factor $K_0^2 = 1-S$ and $S = N(E_F)\Omega U_{\text{eff}}$. As S approaches unity, the Stoner enhancement becomes pronounced and χ increases sharply. Coexistence of electron-electron correlations and ferromagnetic spin fluctuations is previously observed in narrow-band system $LaNiO_3$, where the ratios $\chi_0/\chi_0(\text{DFT})$ and $\gamma/\gamma(\text{DFT})$ are 10.3 and 4.2, respectively [33].

As indicated in the DOS of Fig. 3(a) from DFT calculation, the electrons in Ru t_{2g} orbitals play a crucial role to determine the transport and magnetic properties in $PbCu_3Ru_4O_{12}$. Substituting Ru provides a means to tune these correlations and the associated physical properties. To explore this, we synthesized a series of Ti-substituted compounds, $PbCu_3Ru_{4-x}Ti_xO_{12}$ ($x = 1.2, 2.0, 2.8, 3.6$), together with the end member $PbCu_3Ti_4O_{12}$. The structural and physical properties of these materials were systematically characterized, as discussed below. All compounds retain the same structure with space group *Im*-3 (No. 204) as that of $PbCu_3Ru_4O_{12}$. The results of Rietveld refinement are summarized in Fig. S1 and Tables S2–S7 [26]. This structural consistency provides an ideal platform to examine the influence of *B*-site substitution on the evolution of physical properties in $PbCu_3Ru_{4-x}Ti_xO_{12}$ ($x = 0, 1.2, 2.0, 2.8, 3.6, 4.0$) series.

$PbCu_3Ti_4O_{12}$ is identified as an antiferromagnetic (AFM) insulator, with a Néel temperature (T_N) of 27 K, as shown in Fig. 4(a). The insulating state is successfully reproduced by DFT calculations assuming G-type AFM ordering [Fig. 3(b)], consistent with the G-type AFM structure previously determined by neutron scattering in $CaCu_3Ti_4O_{12}$ [19]. The $\chi(T)$ above T_N follows the Curie-Weiss (C-W) law, $1/\chi = (T-\theta_W)/C$, as shown in Fig. 4(b), yielding a Curie constant (C) of 1.51 and a Weiss temperature (θ_W) of –26.6 K. The effective moment (μ_{eff}), calculated from C, is 1.16 μ_B/Cu. This value is smaller than the theoretical spin-only moment of Cu^{2+} ($S = 1/2$, 1.73 μ_B), but is comparable to that reported for $CaCu_3Ti_4O_{12}$ ($\mu_{\text{eff}} = 1.3$ μ_B/Cu) [10]. The negative θ_W indicates antiferromagnetic interactions in $PbCu_3Ti_4O_{12}$, with $|\theta_W|$ nearly equal to T_N. Antiferromagnetic ordering persists in the Ti-rich region ($x = 4.0, 3.6, 2.8$), with the T_N gradually suppressed from 27 K to 6.5 K as the Ru content increases. The insulating behavior remains at low temperatures for samples with $x = 2.8, 3.6, 4.0$, as shown in Fig. 4(c). The activation energy (E_a), obtained from Arrhenius fits of $\rho(T)$ at high temperatures, as shown in Fig. 4(d), decreases significantly with increasing Ru content [inset of Fig. 4(d)], suggesting that the band gap energy ($\approx 2E_a$) is strongly modified by *B*-site substitution. The nonlinear behavior observed at low temperatures suggests that the electron transport is governed by variable-range hopping (VRH) conduction arising from localized states. The log ρ versus $T^{-1/4}$ plot is shown in Fig. S4. Over the entire measured temperature range, the resistivity follows the $T^{-1/4}$ scaling very well, indicating that three-dimensional Mott VRH dominates the electron transport in samples with $x = 2.8, 3.6, 4.0$.

λ-shaped anomalies in $C_p(T)$ are clearly observed at T_N for $PbCu_3Ru_{4-x}Ti_xO_{12}$ ($x = 2.8$, 3.6, 4.0), becoming broader and shifting to lower temperatures with decreasing Ti

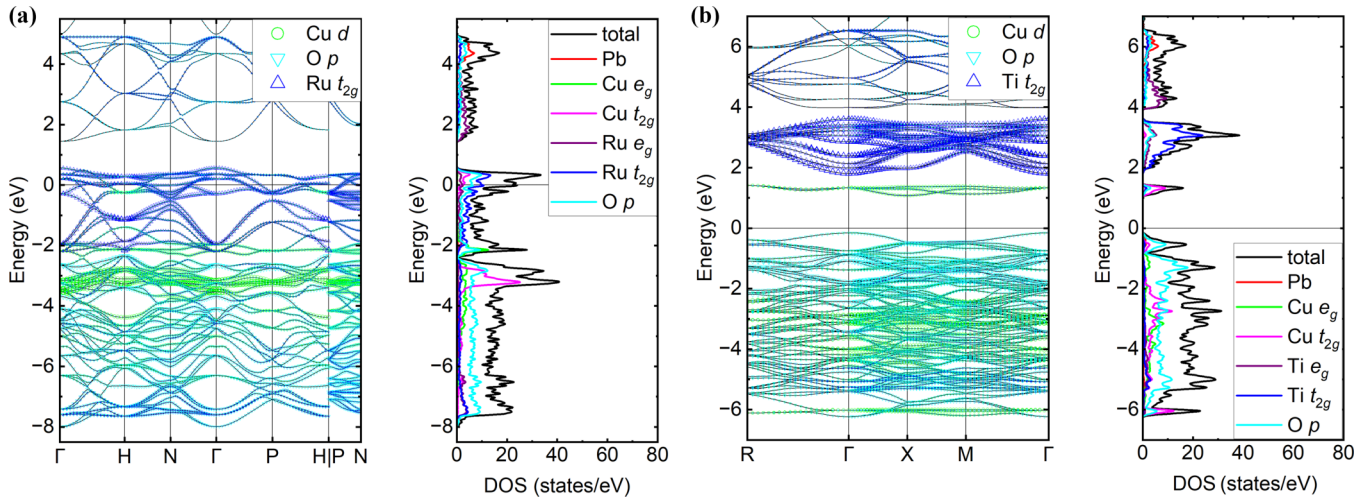

FIG. 3. The band structure (left) and DOS (right) for (a) $PbCu_3Ru_4O_{12}$ and (b) $PbCu_3Ti_4O_{12}$.

content [Fig. 4(e)]. Moreover, Ru^{4+} is likely to contribute to the magnetic properties of $PbCu_3Ru_{4-x}Ti_xO_{12}$ ($x = 2.8, 3.6$). For comparison, the simple perovskite $SrRuO_3$ with Ru^{4+} exhibits a saturation moment of 1.10 μ_B/Ru along the easy axis [34]. As previously proposed for $CaCu_3Ti_4O_{12}$, hybridization involving Ti $3d$ orbitals enables antiferromagnetic superexchange interactions. This mechanism is responsible for the AFM ordering observed in $PbCu_3Ti_4O_{12}$ and also dominates in the $PbCu_3Ru_{4-x}Ti_xO_{12}$ ($x = 2.8, 3.6$) [19].

Figure 4(f) shows the temperature dependence of thermal conductivity for the insulating compositions $PbCu_3Ru_{4-x}Ti_xO_{12}$ ($x = 2.8$, 3.6, 4.0). Owing to the insulating nature of these compounds, the thermal conductivity is dominated by phonon transport. Near room

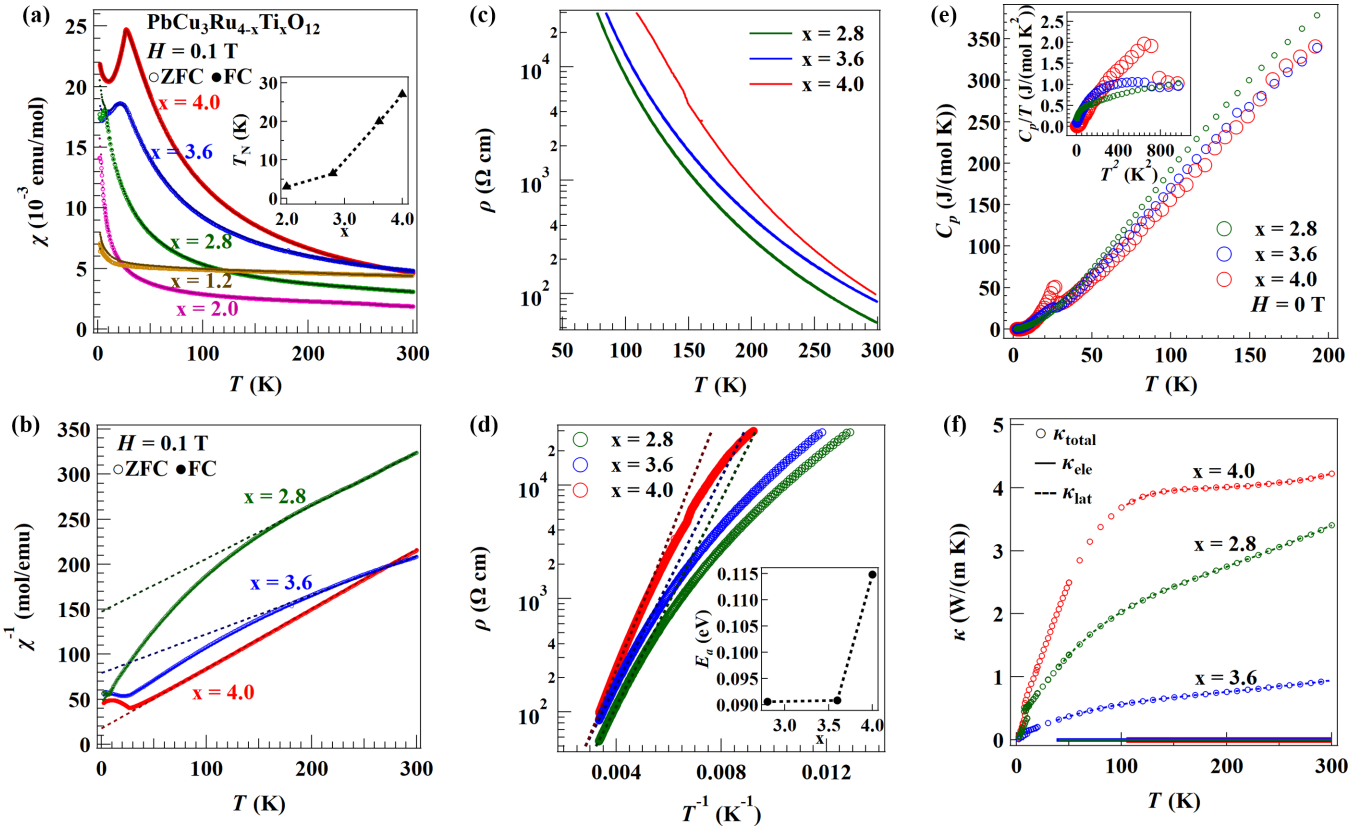

FIG. 4. Temperature dependence of (a) magnetic susceptibility $\chi(T)$ measured under $H = 0.1$ T for $PbCu_3Ru_{4-x}Ti_xO_{12}$ ($x = 1.2, 2.0, 2.8, 3.6, 4.0$), (b) inverse susceptibility $\chi^{-1}(T)$ for $PbCu_3Ru_{4-x}Ti_xO_{12}$ ($x = 2.8, 3.6, 4.0$), (c) resistivity $\rho(T)$ for $PbCu_3Ru_{4-x}Ti_xO_{12}$ ($x = 2.8, 3.6, 4.0$) at $H = 0$ T, (d) Arrhenius plots of ρ vs T^{-1} with activation energy (E_a) deduced from the linear fits shown in inset, (e) specific heat $C_p(T)$ with C_p/T vs T^2 shown in the inset, and (f) thermal conductivity $\kappa(T)$.

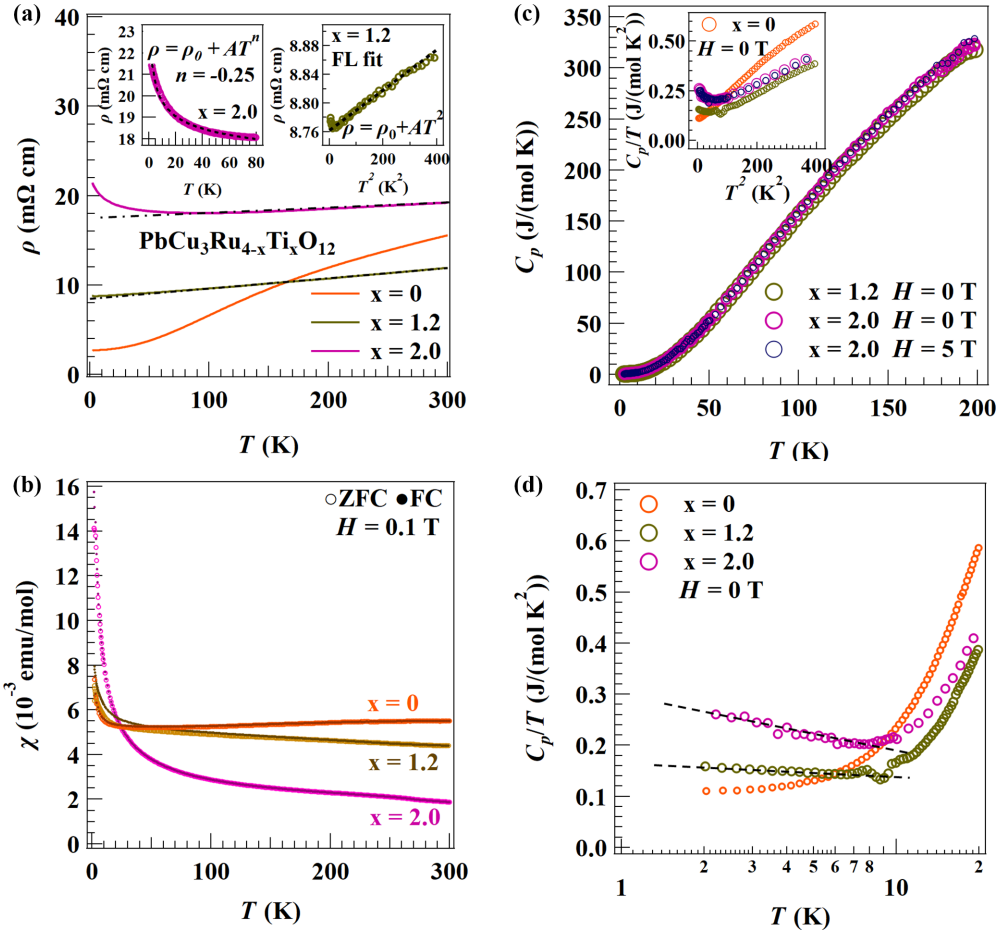

FIG. 5. Temperature dependence of (a) resistivity $\rho(T)$ at $H = 0$ T, (b) magnetic susceptibility $\chi(T)$ measured under $H = 0.1$ T, (c) specific heat $C_p(T)$ with C_p/T versus T^2 shown in the inset, and (d) C_p/T as a function of $\log(T)$. The dashed lines in (a) are provided as guides for the eye.

temperature, the κ values of these polycrystalline samples are comparable to those reported for disordered crystals and approach the minimum thermal conductivity defined by David G. Cahill *et al.* [35]. This observation indicates that phonon scattering is within the interatomic level, suggesting that grain size is not the primary factor governing κ in these compounds. On the other hand, κ remains highly sensitive to microstructural features. In particular, a small difference in sample density or porosity can significantly modify the strength of phonon scattering at grain boundaries [36–38]. Although $PbCu_3Ru_{4-x}Ti_xO_{12}$ ($x = 2.8$, 3.6, 4.0) exhibits comparable κ values over the measured temperature range, slight differences are still observed. These variations are most likely associated with composition-dependent differences in densification during sample synthesis. This conclusion is further supported by the fact that the pristine $PbCu_3Ti_4O_{12}$ sample is markedly denser than the other compositions. Furthermore, SEM images reveal a clear difference in grain-boundary morphology and porosity among the $PbCu_3Ru_{4-x}Ti_xO_{12}$ ($x = 2.8$, 3.6, 4.0) samples (Fig. S5 [26]), supporting the microstructural origin of the observed κ variations.

With further decreasing Ti content, both the antiferromagnetism and insulating behavior are progressively suppressed. The compound $PbCu_3Ru_{4-x}Ti_xO_{12}$ ($x = 2.0$) exhibits a metal-insulator-like transition upon cooling, with the resistivity reaching a minimum at approximately 100 K, as shown in Fig. 5(a). However, in contrast to insulators $PbCu_3Ru_{4-x}Ti_xO_{12}$ ($x = 2.8$, 3.6, 4.0), the subsequent rise in resistivity for $x = 2.0$ below the minimum is weakly temperature-dependent. Specifically, the resistivity increases by only 19% between 100 and 1.8 K, while in more Ti-rich samples it rises by several orders of magnitude. The estimated residual-resistivity ratio (RRR) between 300 and 100 K for $x = 2.0$ is merely 1.06, significantly smaller than that of $PbCu_3Ru_4O_{12}$ (RRR = 5.82). These transport properties indicate that $PbCu_3Ru_{4-x}Ti_xO_{12}$ ($x = 2.0$) remains conductive.

The magnetic susceptibility of the $x = 2.0$ sample increases gradually upon cooling down to $\sim$ 100 K, followed by a more rapid increase at lower temperatures. This χ_0 is smaller than that of the antiferromagnetic samples ($x = 2.8$, 3.6, 4.0) across the entire temperature range, and also smaller than that of $PbCu_3Ru_4O_{12}$, as shown in Figs. 4(a) and 5(b). Unlike samples with $x = 2.8$, 3.6, and 4.0, the antiferromagnetic transition is absent in $\chi(T)$ for $PbCu_3Ru_{4-x}Ti_xO_{12}$ ($x = 2.0$). A bifurcation between the ZFC and FC curves appears below 3 K. The isothermal magnetization measured at 2 K exhibits nonlinear behavior (Fig. S6 [26]), consistent with this bifurcation. A similar feature is observed in samples with $x = 2.8$ and 3.6, with the ZFC-FC bifurcation temperature decreasing

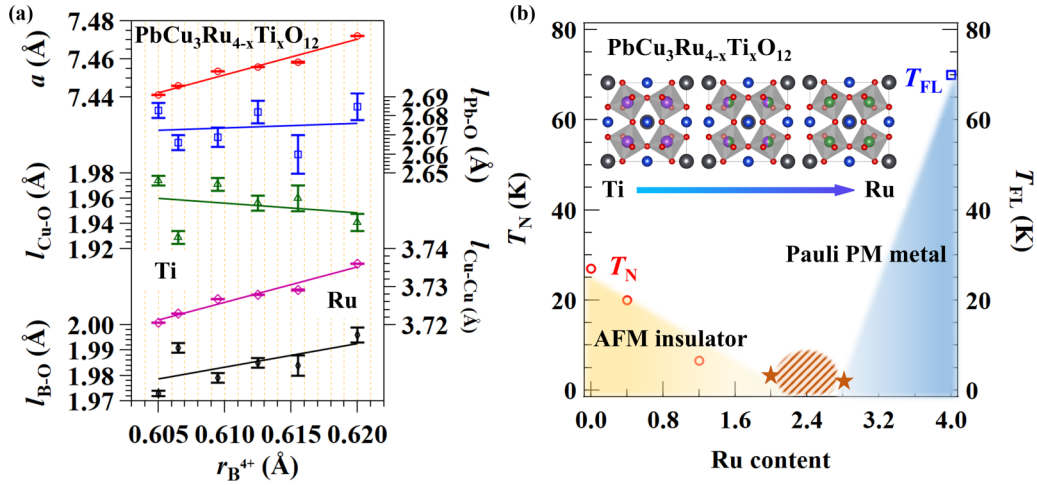

FIG. 6. (a) Structural parameters of $PbCu_3Ru_{4-x}Ti_xO_{12}$ ($x = 0$, 1.2, 2.0, 2.8, 3.6, 4.0) plotted as a function of the average B-site ionic radius. (b) Phase diagram of $PbCu_3Ru_{4-x}Ti_xO_{12}$ ($x = 0$, 1.2, 2.0, 2.8, 3.6, 4.0) as a function of Ru content.

systematically from $\sim$ 15 K ($x = 3.6$) to $\sim$ 6.6 K ($x = 2.8$) and $\sim$ 3 K ($x = 2.0$). This systematic shift with increasing B-site substitution suggests that the bifurcation is unlikely to arise from a specific magnetic impurity, but may instead indicate short-range magnetic ordering. $CaCu_3Ti_{4-x}Ru_xO_{12}$ was demonstrated to exhibit a spin-glass-like transition for $0.5 \leqslant x \leqslant 2.5$ at a constant temperature ($\sim$ 8 K) [39]. In contrast, for $PbCu_3Ru_{4-x}Ti_xO_{12}$, as reported in this study, the bifurcation occurs in a B-site-substitution-dependent manner rather than at a constant temperature, as in $CaCu_3Ti_{4-x}Ru_xO_{12}$. The nature of this bifurcation in $PbCu_3Ru_{4-x}Ti_xO_{12}$ requires further investigation to clarify possible mechanisms, including spin glass, cluster glass, or phase separation.

With further increasing Ru content, metallic behavior is recovered in $PbCu_3Ru_{4-x}Ti_xO_{12}$ ($x = 1.2$), where the resistivity exhibits an almost linear temperature dependence across the entire temperature range, as shown in Fig. 5(a). The $\rho(T)$ data can be fitted with $\rho = \rho_0 + A \times T$, yielding $\rho_0 = 8.76$ mΩ cm and $A = 2.82 \times 10^{-7}$ Ω cm K^{-2}. A small deviation from linearity appears below $\sim$ 47 K, where the data below 20 K can be described by Fermi-liquid behavior [Fig. 5(a), inset]. Interestingly, the $C_p/T - T^2$ data for $x = 1.2$ and 2.0 display a clear upturn below 10 K, continuing to rise down to 2 K, as shown in the inset of Fig. 5(c). This behavior is in sharp contrast to that of $PbCu_3Ru_4O_{12}$ and the antiferromagnetic samples ($x = 2.8$, 3.6, 4.0), which do not show such an upturn. Similar phenomena have been observed in $LaCu_3Ru_xTi_{4-x}O_{12}$ with $x = 2.5$ and 3.0, where these compositions lie in a regime where both the coherent heavy-fermion state and Fermi-liquid behavior break down [40]. Moreover, C_p/T for the $x = 1.2$ and 2.0 samples is proportional to $\log(T)$ ($\log_{10}$, the same below) below 10 K [Fig. 5(d)], a hallmark of Fermi-liquid breakdown [41]. The coexistence of the low-temperature upturn and the $\log(T)$ dependence points to proximity to a QCP [9,41–43]. A logarithmic divergence of the electronic specific heat coefficient γ at the QCP has been observed in compounds such as $YbRh_2Si_2$ and $CeCu_{5.9}Au_{0.1}$ [1,3]. In the Fermi-liquid regime, γ at zero temperature is directly related to the effective mass of Landau quasiparticles. Therefore the divergence of γ near to zero temperature indicates that the quasiparticle effective mass diverges as the system approaches the QCP [4]. Note that the $PbCu_3Ru_{4-x}Ti_xO_{12}$ ($x = 1.2$) sample contains a minor RuO_2 impurity phase, as identified by structure refinement (Fig. S1 [26]). C_p (T) measurements are relatively insensitive to small impurity fractions, whereas resistivity is more susceptible. Thus the C_p (T) results for $PbCu_3Ru_{4-x}Ti_xO_{12}$ ($x = 1.2$ and 2.0) provide reliable evidence that the effective Fermi temperature approaches zero ($T_F \sim 0$ K). Taken together, the breakdown of Fermi-liquid behavior and nearly linear $\rho(T)$ demonstrate that $PbCu_3Ru_{4-x}Ti_xO_{12}$ ($x = 1.2$ and 2.0) are located in close proximity to a QCP.

IV. DISCUSSION

Based on the crystal structure and physical properties of $PbCu_3Ru_{4-x}Ti_xO_{12}$ ($x = 0$, 1.2, 2.0, 2.8, 3.6, 4.0) discussed above, the structural evolution and phase diagram are shown in Figs. 6(a) and 6(b). On the Ru-rich side, the system stabilizes as a Pauli paramagnetic (PM) metal, whereas on the Ti-rich side, it evolves into an antiferromagnetic insulator. The compounds with $x = 1.2$ and 2.0 fall at the boundary between these two regimes, where the resistivity exhibits only weak temperature dependence and no long-range magnetic order is observed down to 1.8 K. The low-temperature upturn in C_p/T versus T indicates the absence of a gap opening in $PbCu_3Ti_{4-x}Ru_xO_{12}$ ($x = 1.2$ and 2.0). Moreover, the linear C_p/T-$\log(T)$ relation resembles the behavior typically associated with a QCP. These results demonstrate that Ti substitution drives the system toward a QCP between $PbCu_3Ru_4O_{12}$ and $PbCu_3Ti_4O_{12}$, as illustrated in Fig. 6(b). The QCP is expected to emerge near 0 K, where B-site substitution continuously suppresses long-range antiferromagnetic order, thereby delineating the boundary between the Fermi-liquid ground state of $PbCu_3Ru_4O_{12}$ and the antiferromagnetic insulating state of $PbCu_3Ti_4O_{12}$. $LaCu_3Ru_xTi_{4-x}O_{12}$ was shown to exhibit a similar physical scenario, in which dilution of Ru^{4+} by nonmagnetic Ti^{4+} in the A-site-ordered perovskite lattice gradually suppresses Kondo-type behavior across the metal-insulator transition [40].

To compare $PbCu_3Ru_4O_{12}$ with its analogue $CaCu_3Ru_4O_{12}$, DFT calculations reveal that both compounds share similar electronic structures and crystallize in the cubic space group *Im*-3 (No. 204). The lattice parameter of $PbCu_3Ru_4O_{12}$ is larger, reflecting the larger ionic radius of Pb^{2+}. In perovskite oxides, *A*-O interactions compete with *B*-site cations for O $2p_\pi$ electrons. A more ionic *A*-site cation interacts weakly with O $2p$ orbitals, allowing stronger covalent mixing between O $2p$ orbital and *B*-site *d* orbitals, which broadens the *B*-O bandwidth. In contrast, the more covalent Pb^{2+} competes effectively for O $2p$ electrons, reducing the *B*-O bandwidth [44]. Additionally, longer *B*-O bonds narrow the bandwidth further. In $PbCu_3Ru_4O_{12}$, the Ru-O bond length (1.996 Å) is longer than that in $CaCu_3Ru_4O_{12}$ (1.981 [8] and 1.966 Å [45]), so the combined effect of stronger Pb^{2+} covalency and elongated Ru-O bonds produces a narrower bandwidth and enhances the DOS at the Fermi level. DFT calculations confirm this trend, with $N(E_F)$ values of 10.58 states/eV/f.u./spin for $PbCu_3Ru_4O_{12}$ and 7.15 states/eV/f.u./spin for $CaCu_3Ru_4O_{12}$. The corresponding γ(DFT) and χ_0(DFT) values are summarized in Table I and compared with experimental values. In both compounds, the ratio χ_0/χ_0(DFT) is significantly larger than γ/γ(DFT), indicating Stoner enhancement. The discovery and investigation of $PbCu_3Ru_4O_{12}$ underscores the importance of Stoner enhancement in Pauli paramagnetic metals within these two *A*-site ordered perovskite oxides, where electron correlations and ferromagnetic spin fluctuations play key roles in determining their physical properties. This aspect was not addressed in previous reports. The Wilson ratio (R_W) reflects the relative magnitudes of χ_0/χ_0(DFT) and γ/γ(DFT). For $PbCu_3Ru_4O_{12}$, R_W is slightly higher than in $CaCu_3Ru_4O_{12}$ and comparable to $LaCu_3Ru_4O_{12}$ ($R_W \sim 3.15$). In $Ca_{1-x}La_xCu_3Ru_4O_{12}$, R_W decreases from $x = 0$ to $x = 0.25$ ($R_W \sim 2.63$), then increases for $x \geqslant 0.5$, inferring a change in electronic states within this compositional range [32]. Future studies on *A*-site substitution in $PbCu_3Ru_4O_{12}$ may similarly provide a route to tune its electronic states. Furthermore, R_W values estimated for $PbCu_3Ru_{4-x}Ti_xO_{12}$ ($x = 1.2$ and 2.0) are 1.9 and 1.4, respectively, in sharp contrast to $ACu_3Ru_4O_{12}$ (A = Pb, Ca, La, and Na), further indicating a significant difference in their electronic state.

V. CONCLUSIONS

In conclusion, we have successfully synthesized a new series of the *A*-site ordered perovskites $PbCu_3Ru_{4-x}Ti_xO_{12}$ ($x = 0$, 1.2, 2.0, 2.8, 3.6, 4) under high-pressure conditions. This system provides a rare platform to trace the evolution from a heavy-fermion metallic state to a long-range antiferromagnetic insulating state. Increasing Ru content progressively suppresses the antiferromagnetic order in $PbCu_3Ti_4O_{12}$, bringing compounds with $x = 1.2$ and 2.0 close to a QCP. The susceptibility maximum in $PbCu_3Ru_4O_{12}$ is well reproduced by the model proposed by Misawa, indicating strong electron correlations and proximity to a magnetic transition toward ferromagnetism. Comparison with $CaCu_3Ru_4O_{12}$, shows that the more covalent nature of Pb^{2+} and longer Ru-O bond length contribute to a narrower bandwidth and a larger $N(E_F)$. This demonstrates that Pb substitution in *A*-site-ordered perovskites offers an effective pathway to tune the electronic structure and, consequently, the physical properties for potential application. Overall, the $PbCu_3Ru_{4-x}Ti_xO_{12}$ series serves as a model system to investigate the interplay between electron correlations, magnetic ordering, and lattice effects in *A*-site ordered perovskite oxides. These materials, along with the ability to tune their microscopic interactions, offer promising opportunities for designing functional oxides with controllable electronic and magnetic properties.

ACKNOWLEDGMENTS

This work is supported in part by the National Natural Science Foundation of China (NSFC) (Grants No. 12174025, No. 12321004, and No. 12204045), the National Key R&D Program of China (Grants No. 2023YFA1406002 and No. 2020YFA0308801), and the Chinese Academy of Sciences Superconducting Research Project (Grant No. SCZX-0101). X.L. acknowledges the support by the Beijing Institute of Technology Research Fund Program (Grant No. 2023CX01027). J.Q. acknowledges the support by the Beijing Institute of Technology Research Fund Program for Young Scholars. M.J. acknowledges the support by Beijing Institute of Technology Laboratory Research Project (Grant No. 2023BITSYB07).

DATA AVAILABILITY

The data that support the findings of this article are not publicly available upon publication because it is not technically feasible and/or the cost of preparing, depositing, and hosting the data would be prohibitive within the terms of this research project. The data are available from the authors upon reasonable request.

[1] H. v. Löhneysen, T. Pietrus, G. Portisch, H. G. Schlager, A. Schröder, M. Sieck, and T. Trappmann, Non-Fermi-liquid behavior in a heavy-fermion alloy at a magnetic instability, Phys. Rev. Lett. **72**, 3262 (1994).

[2] A. Schröder, G. Aeppli, R. Coldea, M. Adams, O. Stockert, H. v. Löhneysen, E. Bucher, R. Ramazashvili, and P. Coleman, Onset of antiferromagnetism in heavy-fermion metals, Nature (London) **407**, 351 (2000).

[3] O. Trovarelli, C. Geibel, S. Mederle, C. Langhammer, F. M. Grosche, P. Gegenwart, M. Lang, G. Sparn, and F. Steglich, $YbRh_2Si_2$: Pronounced non-Fermi-liquid effects above a low-lying magnetic phase transition, Phys. Rev. Lett. **85**, 626 (2000).

[4] P. Gegenwart, Q. Si, and F. Steglich, Quantum criticality in heavy-fermion metals, Nat. Phys. **4**, 186 (2008).

[5] H. A. Krug von Nidda, R. Bulla, N. Bttgen, M. Heinrich, and A. Loidl, Heavy fermions in transition metals and transition-metal oxides, European Physical J. B - Condensed Matter **34**, 399 (2003).

[6] S. Kondo, D. C. Johnston, C. A. Swenson, F. Borsa, A. V. Mahajan, L. L. Miller, T. Gu, A. I. Goldman, M. B. Maple, D.

A. Gajewski, *et al.*, LiV_2O_4: A heavy fermion transition metal oxide, Phys. Rev. Lett. **78**, 3729 (1997).

[7] S. Nakatsuji, Y. Machida, Y. Maemo, T. Tayama, T. Sakakibara, J. van Duijn, L. Balicas, J. N. Millican, R. T. Macaluso, and J. Y. Chan, Metallic spin-liquid behavior of the geometrically frustrated kondo Lattice $Pr_2Ir_2O_7$, Phys. Rev. Lett. **96**, 087204 (2006).

[8] A. Krimmel, A. Günther, W. Kraetschmer, H. Dekinger, N. Büttgen, A. Loidl, S. G. Ebbinghaus, E. W. Scheidt, and W. Scherer, Non-Fermi-liquid behavior in $CaCu_3Ru_4O_{12}$, Phys. Rev. B **78**, 165126 (2008).

[9] J. G. Cheng, J. S. Zhou, Y. F. Yang, H. D. Zhou, K. Matsubayashi, Y. Uwatoko, A. MacDonald, and J. B. Goodenough, Possible kondo physics near a metal-insulator crossover in thea-site ordered perovskite $CaCu_3Ir_4O_{12}$, Phys. Rev. Lett. **111**, 176403 (2013).

[10] W. Kobayashi, I. Terasaki, J.-i. Takeya, I. Tsukada, and Y. Ando, A novel heavy-fermion state in $CaCu_3Ru_4O_{12}$, J. Phys. Soc. Jpn. **73**, 2373 (2004).

[11] S. Tanaka, N. Shimazui, H. Takatsu, S. Yonezawa, and Y. Maeno, Heavy-mass behavior of ordered perovskites A $Cu_3Ru_4O_{12}$ (A = Na, Ca, La), J. Phys. Soc. Jpn. **78**, 024706 (2009).

[12] M. Mizumaki, T. Mizokawa, A. Agui, S. Tanaka, H. Takatsu, S. Yonezawa, and Y. Maeno, Oxygen hole state in a-site ordered perovskite A $Cu_3Ru_4O_{12}$(A = Na, Ca, and La) probed by resonant x-ray emission spectroscopy, J. Phys. Soc. Jpn. **82**, 024709 (2013).

[13] D. Takegami, C. Y. Kuo, K. Sakebayashi, J. G. Kim, C. F. Chang, C. E. Liu, C. N. Wu, D. Kasinathan, S. G. Altendorf, K. Hoefer, *et al.*, $CaCu_3Ru_4O_{12}$: A high-kondo-temperature transition-metal oxide, Phys. Rev. X **12**, 011017 (2022).

[14] H. Kato, T. Tsuruta, M. Matsumura, T. Nishioka, H. Sakai, Y. Tokunaga, S. Kambe, and R. E. Walstedt, Temperature-induced change in the magnitude of the effective density of states: A NQR/NMR study of the a-site-ordered perovskite system $CaCu_3Ru_4O_{12}$, J. Phys. Soc. Jpn. **78**, 054707 (2009).

[15] Y. Shimakawa, Crystal and magnetic structures of $CaCu_3Fe_4O_{12}$ and $LaCu_3Fe_4O_{12}$: Distinct charge transitions of unusual high valence Fe, J. Phys. D Appl. Phys. **48**, 504006 (2015).

[16] Z. Zeng, M. Greenblatt, M. A. Subramanian, and M. Croft, Large low-field magnetoresistance in perovskite-type $CaCu_3Mn_4O_{12}$ without double exchange, Phys. Rev. Lett. **82**, 3164 (1999).

[17] D. Meyers, S. Mukherjee, J. G. Cheng, S. Middey, J. S. Zhou, J. B. Goodenough, B. A. Gray, J. W. Freeland, T. Saha-Dasgupta, and J. Chakhalian, Zhang-Rice physics and anomalous copper states in A-site ordered perovskites, Sci. Rep. **3**, 1834 (2013).

[18] H. Shiraki, T. Saito, T. Yamada, M. Tsujimoto, M. Azuma, H. Kurata, S. Isoda, M. Takano, and Y. Shimakawa, Ferromagnetic cuprates $CaCu_3Ge_4O_{12}$ and $CaCu_3Sn_4O_{12}$ with A-site ordered perovskite structure, Phys. Rev. B **76**, 140403(R) (2007).

[19] Y. J. Kim, S. Wakimoto, S. M. Shapiro, P. M. Gehring, and A. P. Ramirez, Neutron scattering study of antiferromagnetic order in $CaCu_3Ti_4O_{12}$, Solid State Commun. **121**, 625 (2002).

[20] G. Kresse and J. Hafner, *Ab initio* molecular dynamics for liquid metals, Phys. Rev. B **47**, 558 (1993).

[21] G. Kresse and J. Furthmüller, Efficient iterative schemes for *ab initio* total energy calculations using a plane-wave basis set, Phys. Rev. B **54**, 11169 (1996).

[22] P. E. Blöchl, Projector augmented-wave method, Phys. Rev. B **50**, 17953 (1994).

[23] J. P. Perdew, K. Burke, and M. Ernzerhof, Generalized gradient approximation made simple, Phys. Rev. Lett. **77**, 3865 (1996).

[24] M. B. Zölfl, T. Maier, T. Pruschke, and J. Keller, Electronic properties of CuO_2-planes: A DMFT study, Eur. Phys. J. B **13**, 47 (2000).

[25] S. Choi, A. Kutepov, K. Haule, M. van Schilfgaarde, and G. Kotliar, First-principles treatment of Mott insulators: Linearized QSGW+DMFT approach, npj Quantum Mater. **1**, 16001 (2016).

[26] See Supplemental Material at http://link.aps.org/supplemental/10.1103/hdnd-sd52 for SXRD refinement result of $PbCu_3Ru_{4-x}Ti_xO_{12}$ system, Magnetic susceptibility $\chi(T)$ measured under $H = 1$ T with Misawa's model fitting, $\log(T) - T^{-1/4}$ plot of insulator samples, SEM image of insulator samples, $M-H$ result of $PbCu_3Ru_{4-x}Ti_xO_{12}$ system under $T = 2$ K and the Feynman's diagram illustrating of mass enhancement and Stoner enhancement.

[27] S. Lee, J. R. Zhang, S. Torii, S. Choi, D.-Y. Cho, T. Kamiyama, J. Yu, K. A. McEwen, and J.-G. Park, Large in-plane deformation of RuO_6 octahedron and ferromagnetism of bulk $SrRuO_3$, J. Phys. Condens. Matter **25**, 465601 (2013).

[28] A. C. Jacko, J. O. Fjærestad, and B. J. Powell, A unified explanation of the Kadowaki–Woods ratio in strongly correlated metals, Nat. Phys. **5**, 422 (2009).

[29] H. Liu, Y. Cao, Y. Xu, D. J. Gawryluk, E. Pomjakushina, S. Y. Gao, P. Dudin, M. Shi, L. Yan, Y. F. Yang, *et al.*, Observation of flat bands due to band hybridization in the 3*d*-electron heavy-fermion compound $CaCu_3Ru_4O_{12}$, Phys. Rev. B **102**, 035111 (2020).

[30] H. C. Jamieson and F. D. Manchester, The magnetic susceptibility of Pd, PdH and PdD between 4 and 300 K, J. Phys. F Met. Phys. **2**, 323 (1972).

[31] S. Misawa, Susceptibility maximum and grand Fermi-liquid effect in 4*d* and 5*d* transition metals, Physica B+C **86-88**, 383 (1977).

[32] T.-H. Kao, H. Sakurai, S. Yu, H. Kato, N. Tsujii, and H.-D. Yang, Origin of the magnetic susceptibility maximum in $CaCu_3Ru_4O_{12}$ and electronic states in the A-site substituted compounds, Phys. Rev. B **96**, 024402 (2017).

[33] J. S. Zhou, L. G. Marshall, and J. B. Goodenough, Mass enhancement versus Stoner enhancement in strongly correlated metallic perovskites: $LaNiO_3$ and $LaCuO_3$, Phys. Rev. B **89**, 245138 (2014).

[34] G. Cao, S. McCall, M. Shepard, J. E. Crow, and R. P. Guertin, Thermal, magnetic, and transport properties of single-crystal $Sr_{1-x}Ca_xRuO_3(0 \leqslant x \leqslant 1.0)$, Phys. Rev. B **56**, 321 (1997).

[35] D. G. Cahill, S. K. Watson, and R. O. Pohl, Lower limit to the thermal conductivity of disordered crystals, Phys. Rev. B **46**, 6131 (1992).

[36] S. Raghavan, H. Wang, R. B. Dinwiddie, W. D. Porter, and M. J. Mayo, The effect of grain size, porosity and yttria content on the thermal conductivity of nanocrystalline zirconia, Scr. Mater. **39**, 1119 (1998).

[37] J. F. Troncoso, P. Chudzinski, T. N. Todorov, P. Aguado-Puente, M. Grüning, and J. J. Kohanoff, The effect of grain

size, porosity and yttria content on the thermal conductivity of nanocrystalline zirconia, Phys. Rev. Mater. **5**, 014604 (2021).

[38] D. S. Smith, F. Puech, B. Nait-Ali, A. Alzina, and S. Honda, Grain boundary thermal resistance and finite grain size effects for heat conduction through porous polycrystalline alumina, Int. J. Heat Mass Transfer **121**, 1273 (2018).

[39] T.-H. Kao, H. Sakurai, S. Yu, H. Kato, N. Tsujii, and H.-D. Yang, Electronic phase transition between localized and itinerant states in the solid-solution system $CaCu_3Ti_{4-x}Ru_xO_{12}$, Phys. Rev. B **95**, 195141 (2017).

[40] S. Riegg, S. Widmann, B. Meir, S. Sterz, A. Günther, N. Büttgen, S. G. Ebbinghaus, A. Reller, H. A. Krug von Nidda, and A. Loidl, Kondo-type behavior of the Ru^{4+} lattice in $LaCu_3Ru_4O_{12}$, Phys. Rev. B **93**, 115149 (2016).

[41] G. Cao, O. Korneta, S. Chikara, L. E. DeLong, and P. Schlottmann, Non-Fermi-liquid behavior in single-crystal $CaRuO_3$: Comparison to ferromagnetic $SrRuO_3$, Solid State Commun. **148**, 305 (2008).

[42] J. Chen, Z. Wang, Y. Li, C. Feng, J. Dai, Z. Xu, and Q. Si, Heavy fermion quantum criticality at dilute carrier limit in $CeNi_{2-\delta}(As_{1-x}P_x)_2$, Sci. Rep. **9**, 12307 (2019).

[43] H. v. Löhneysen, Non-Fermi-liquid behaviour in the heavy-fermion system $CeCu_{6-x}Au_x$, J. Phys. Condens. Matter **8**, 9689 (1996).

[44] C. Q. Jin, J. S. Zhou, J. B. Goodenough, Q. Q. Liu, J. G. Zhao, L. X. Yang, Y. Yu, R. C. Yu, T. Katsura, A. Shatskiy, *et al.*, High-pressure synthesis of the cubic perovskite $BaRuO_3$ and evolution of ferromagnetism in $ARuO_3$ (A = Ca, Sr, Ba) ruthenates, Proc. Natl. Acad. Sci. USA **105**, 7115 (2008).

[45] C. de la Calle, J. Sánchez-Benítez, F. Barbanson, N. Nemes, M. T. Fernández-Díaz, and J. A. Alonso, Transition from Pauli-paramagnetism to ferromagnetism in $CaCu_3(Ru_{4-x}Mn_x)O_{12}$ ($0 \leqslant x \leqslant 3$) perovskites, J. Appl. Phys. **109**, 123914 (2011).